Articles

Role of the His57−Glu214 Ionic Couple Located in the Active Site of *Mycobacterium tuberculosis* FprA[†,‡]

Andrea Pennati,[§] Adelia Razeto,[||] Matteo de Rosa,[§] Vittorio Pandini,[§] Maria Antonietta Vanoni,[§] Andrea Mattevi,[||] Alessandro Coda,[||] Alessandro Aliverti,*[,§] and Giuliana Zanetti[§]

Dipartimento di Scienze Biomolecolari e Biotecnologie, Università degli Studi di Milano, via Celoria 26, 20133 Milano, Italy, and Dipartimento di Genetica e Microbiologia, Università degli Studi di Pavia, Via Ferrata 1, 27100 Pavia, Italy

Received February 22, 2006; Revised Manuscript Received May 19, 2006

ABSTRACT: *Mycobacterium tuberculosis* FprA is a NADPH-ferredoxin reductase, functionally and structurally similar to the mammalian adrenodoxin reductase. It is presumably involved in supplying electrons to one or more of the pathogen's cytochrome P450s through reduced ferredoxins. It has been proposed on the basis of crystallographic data (Bossi, R. T., et al. (2002) *Biochemistry 41*, 8807−8818) that the highly conserved His57 and Glu214 whose side chains are H-bonded are involved in catalysis. Both residues were individually changed to nonionizable amino acyl residues through site-directed mutagenesis. Steady-state kinetics showed that the role of Glu214 in catalysis is negligible. On the contrary, the substitutions of His57 markedly impaired the catalytic efficiency of FprA for ferredoxin in the physiological reaction. Furthemore, they decreased the k_{cat}/K_m value for NADPH in the ferricyanide reduction. Rapid-reaction (stopped-flow) kinetic analysis of the isolated reductive half-reaction of wild-type and His57Gln forms of FprA with NADPH and NADH allowed a detailed description of the mechanism of enzyme-bound FAD reduction, with the identification of the intermediates involved. The His57Gln mutation caused a 6-fold decrease in the rate of hydride transfer from either NADPH or NADH to the enzyme-bound FAD cofactor. The 3D structure of FprA−H57Q, obtained at 1.8 Å resolution, explains the inefficient hydride transfer of the mutant in terms of a suboptimal geometry of the nicotinamide−isoalloxazine interaction in the active site. These data demonstrate the role of His57 in the correct binding of NADPH to FprA for the subsequent steps of the catalytic cycle to proceed at a high rate.

Ferredoxin-NADP$^+$ reductases (FNR[1], EC 1.18.1.2) are a large family of FAD-containing oxidoreductases that catalyze the reversible electron transfer between NADP(H) and ferredoxins (*1*, *2*). They can be classified in two evolutionary unrelated subgroups: the plant-type FNRs, whose prototype is the chloroplast enzyme (*3*), and the glutathione reductase (GR)-type FNRs. The best known member of GR-type FNRs is the mammalian adrenodoxin reductase (AdR), which participates in steroid hormone biosynthesis in adrenal glands by forming a short electron transport chain that conveys the reducing power from NADPH to cytochrome P450s via adrenodoxin (*4*, *5*). In addition, AdR and adrenodoxin have a general role in iron−sulfur cluster biogenesis (*6*). The *Saccharomyces cerevisiae* Arh1 and Yah1 homologues of AdR and adrenodoxin have been shown to be essential (*7*, *8*). Mycobacteria are among the few prokaryotes that possess AdR-like enzymes, which are encoded by *fprA* and *fprB* genes (*9*). FprA, which displays 41% sequence identity with AdR, shares several functional properties with the mammalian homologue (*10*).

Structure−function relationships in plant-type FNRs have been extensively studied by the combined approaches of site-directed mutagenesis and X-ray crystallography, providing a comprehensive picture of their catalytic mechanism (*11*, *12*). The X-ray structures of the complexes of *M. tuberculosis* FprA with either NADP$^+$ or NADPH have been recently obtained at up to 1.05 Å resolution (*13*), complementing and extending the structural information available for mammalian AdR (*14*−*16*). As found for plant-type FNRs, the active site of AdR and FprA is located at the interface between the two

[†] This work was supported by grants from Ministero dell'Istruzione, dell'Università e della Ricerca of Italy (Prin 2003) and Fondazione Cariplo, Milano, Italy.

[‡] The coordinates of the FprA-H57Q structure have been deposited in the Protein Data Bank with accession code 2C7G.

* Corresponding author. Tel: +39 02 50314897. Fax: +39 02 50314895. E-mail: alessandro.aliverti@unimi.it.

[§] Università degli Studi di Milano.

[||] Università degli Studi di Pavia.

[1] Abbreviations: FNR, ferredoxin-NADP$^+$ reductase; GR, glutathione reductase; AdR, adrenodoxin reductase; NADPO, 3-carboxamide-4-piridone adenine dinucleotide phosphate; Fd I, spinach leaf ferredoxin I; IPTG, isopropyl-β-D-thiogalactopyranoside; DTT, dithiothreitol; E_m, midpoint redox potential; CT1, charge-transfer complex between enzyme-bound FAD and NADPH or NADH; CT2, charge-transfer complex bewteen enzyme-bound FADH$^-$ and NADP$^+$; SQ, semiquinone species of FprA-bound FAD.

10.1021/bi060369m CCC: $33.50
Published on Web 06/28/2006

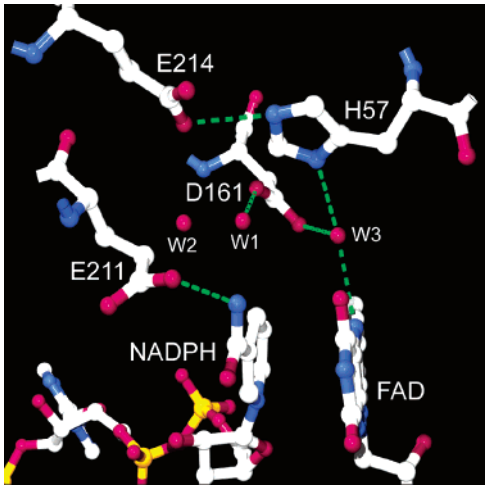

FIGURE 1: Ordered water molecules in the active site of FprA. Ball and stick representation of the active-site region of the complex between FprA and NADPH (pdb entry 1LQU) (*13*). Water molecules are indicated as W1, W2, and W3. H bonds are represented as green dashed lines. The model has been drawn using Swiss-PDBViewer 3.7 (http://www.expasy.org/spdbv) and POV-Ray 3.6 (Persistence of Vision Raytracer Pty., Ltd.).

domains of the protein. However, the interdomain interactions are much looser, and the two domains are more mobile in GR-type FNRs with respect to plant-type FNRs (*12*, *15*, *16*). Various proposals on the involvement of specific residues in the catalytic mechanism of GR-type FNRs have been made on the basis of crystallographic data. However, such hypotheses have never been tested by mutagenesis studies, with the exception of a study on the involvement of AdR basic residues in adrenodoxin binding (*17*).

In this article, we report the properties of mutant FprA forms where His57 and Glu214, which correspond to His55 and Glu212 of bovine AdR, respectively, were individually changed to uncharged residues. His57 and Glu214 are located in the active center of FprA with their side chains at H-bonding distance and presumably forming an ion pair. His57, together with other residues such as Asp161, could play a role in catalysis in this class of enzymes by holding water molecules in place (Figure 1). These molecules (w1 and w3) in turn may favor the hydride transfer between NADPH and FAD by polarizing the C4 position of the nicotinamide and the N5 position of the isoalloxazine moieties. His57 and Glu214 have been proposed to be implicated in the activation of water 1, which initiates the oxidation of $NADP^+$ to 3-carboxamide-4-piridone adenine dinucleotide phosphate (NADPO) in an unusual side reaction catalyzed by FprA (*13*). Furthermore, the side chain of His55 of AdR has been proposed to stabilize the neutral (blue) FAD semiquinone (SQ) (*14*) and to favor the proton transfer from the FAD semiquinone to the active-site central water molecule during the enzyme catalytic cycle (*15*). The altered functional properties of the most interesting mutant, FprA−H57Q, were interpreted on the basis of its 3D structure, which was determined by X-ray crystallography.

MATERIALS AND METHODS

Materials. $NADP^+$ and NADPH were purchased from Sigma. Horse heart cytochrome *c* (Sigma) was further purified by cation-exchange chromatography on SP-Sepharose (Amersham). Restriction enzymes were obtained from Amersham, and factor X_a from Pierce. *Mycobacterium smegmatis* FdxA and recombinant spinach leaf ferredoxin I (Fd I) were purified as described previously (*10*, *18*). All other chemicals were of the highest grade.

Site-Directed Mutagenesis and Plasmid Construction. The amino acyl replacements were introduced in the gene-encoding FprA, using the QuikChange site-directed mutagenesis kit (Stratagene) and the plasmid pET*fprA* (*10*) as the template. The following couples of complementary oligonucleotides were used (base changes are underlined): Glu214Ala, 5′-CGTTGGAGTTGCGCGCGCTGGCCGACCTCG-3′ and 5′-CGAGGTCGGCCAGCGCGCGCAACTCCAACG-3′; His57Ala, 5′-GTCGCGCCGGATGCGCCCAAGATCAAGTCG-3′ and 5′-CGACTTGATCTTGGGCGCATCCGGCGCGAC-3′; His57Gln, 5′-GTCGCGCCGGATCAGCCCAAGATCAAGTCG-3′ and 5′-CGACTTGATCTTGGGCTGATCCGGCGCGAC-3′. The entire *fprA* insert of all of the plasmids thus obtained was sequenced and then recloned in the *Nde*I site of pET28b (Novagen) to yield plasmids pETHis*fprA*, pETHis*fprA*-E214A, pETHis*fprA*-H57A, and pETHis*fprA*-H57Q, respectively, which express the proteins with an *N*-terminal His-tag.

Recombinant Gene Expression and Protein Purification. *Escherichia coli* HMS174(DE3) transformed cells were grown to mid-exponential phase at 25 °C under agitation in 2×YT medium supplemented with 30 mg/L of kanamycin. The expression of the *fprA* forms was induced with 0.1 mM IPTG for 15−17 h at 16 °C. The *E. coli* cells were disrupted by sonication in 50 mM sodium phosphate at pH 8.0, containing 300 mM NaCl, 10% glycerol, 10 mM imidazole, and 1 mM β-mercaptoethanol (buffer A) supplemented with 1 mM phenylmethylsulfonyl fluoride. After centrifugation, the supernatant was loaded on a Ni-NTA Agarose (Qiagen) column equilibrated in buffer A. The FprA forms were eluted with 250 mM imidazole in buffer A. Both FprA mutants at position 57 that still contained significant amounts of NADPO at this stage were further purified by affinity chromatography on 2′,5′ADP Sepharose 4B (Amersham), using a pulse of 200 mM NaCl in 50 mM HEPES−NaOH at pH 7.0, containing 10% glycerol and 1 mM DTT. After concentration and desalting, the enzymes were stored at −20 °C in 50 mM HEPES−NaOH at pH 7.0, containing 100 mM NaCl, 10% glycerol, and 1 mM DTT.

Spectral Analyses, Thermal Inactivation, and Steady-State Kinetics. Absorption spectra were recorded on an Agilent 8453 diode-array spectrophotometer. The extinction coefficient of the protein-bound flavin was determined by quantitating the FAD released from the apoprotein following SDS treatment (*19*). To study thermal unfolding, the FprA solutions (10 μM) in 10 mM HEPES−NaOH at pH 7.0 containing 100 mM NaCl and 10% glycerol were incubated at different temperatures in the 35−50 °C range. At particular time intervals, the residual NADPH−ferricyanide reductase activity was measured. The steady-state kinetic parameters of the FprA forms were determined for both the $K_3Fe(CN)_6$ reductase and the ferredoxin-dependent cytochrome *c* reductase activities using either NADPH or NADH as the reductant in 100 mM Tris-HCl at pH 8.2, as previously described (*10*). Initial velocity data were fitted to the equation for a ping−pong bi−bi mechanism by nonlinear regression.

Active-Site Titrations and Analysis of the Redox Properties of FprA-Bound FAD. Titrations of the FprA forms (ca. 15

μM) with either $NADP^+$ or NAD^+ were performed spectrophotometrically at 16 °C in 20 mM HEPES−NaOH at pH 7.0, containing 10% glycerol using a Cary 100 (Varian) double-beam spectrophotometer. In the case of titrations with $NADP^+$, the mixtures also included 300 mM NaCl. The K_d values were obtained by fitting data sets by nonlinear regression to the theoretical equation for a 1:1 binding (*20*). A spectral analysis of the FprA forms in different redox states was performed by stepwise anaerobic reduction of the enzymes by the light/EDTA system (*21*) at 16 °C. The enzyme forms were diluted to 16−22 μM in 10 mM HEPES−NaOH at pH 7.0, containing 100 mM NaCl, 10% glycerol, 15 mM EDTA, and 1.4 μM 5-deazariboflavin. When present, $NADP^+$ was in a 1.2 molar ratio with respect to the enzyme. The redox potential of FprA and FprA−H57Q was determined at 16 °C by stepwise anaerobic photoreduction of 10−15 μM enzyme solutions in 100 mM phosphate−NaOH at pH 7.0, containing 10% glycerol, 15 mM EDTA, and 1.4 μM 5-carba-5-deazariboflavin. Both benzyl viologen ($E_m = -359$ mV, $n = 1$) and methyl viologen ($E_m = -440$ mV, $n = 1$) (*22*) (0.5−1.0 μM each) were included as electron mediators and either 15−20 μM antraquinone-2,6-disulfonate ($E_m = -184$ mV, $n = 2$) or antraquinone-2-sulfonate ($E_m = -225$ mV, $n = 2$) (*22*) as redox indicators. The absorbance values at either 354 nm (isosbestic point for the reduction of antraquinone-2,6-disulfonate) or 355 nm (isosbestic point for the reduction of antraquinone-2-sulfonate) were used to monitor the reduction FAD. The absorbance values at 338 or 336 nm (isosbestic points for the FAD_{ox}/FAD_{red} couple of FprA and FprA−H57Q, respectively) were used to monitor the reduction of the indicator dye. Data were fitted to the Nernst equation to obtain the E_m value of the FAD bound to the FprA forms.

Rapid Kinetics. Rapid-reaction studies of the enzyme reductive half-reaction were performed under anaerobic conditions using a Hi-Tech Scientific SF-61 DX2 stopped-flow spectrophotometer equipped with a diode-array detector (300−700 nm). The enzyme forms (ca. 30 μM, before mixing) were reacted with various concentrations of either NADH or NADPH at 25 °C in 50 mM HEPES−NaOH at pH 7.0, containing 100 mM NaCl, 10% glycerol. The absorbance traces at individual wavelengths were analyzed using KinetAsyst 3 software (Hi-Tech Scientific). A global analysis of multiwavelength kinetic data sets was performed with Specfit/32 version 3.0 (Spectrum Software Associates, Chapel Hill, NC).

Crystallization. Recombinant FprA−H57Q was crystallized by vapor diffusion in sitting drops. The enzyme solution was mixed in a 1:1 ratio with well solutions. The enzyme (25 mg/mL) was in 50 mM HEPES−NaOH at pH 7.0, containing 100 mM NaCl, 10% glycerol, 5 mM DTT, and 0.65 mM $NADP^+$. The well solutions consisted of 30% (w/v) poly(ethylene glycol) 4000, 0.1 M sodium citrate at pH 5.6, and 0.2 M ammonium acetate. Crystals grow under these conditions in approximately 3−4 weeks. They are very small cubes of $0.05 \times 0.05 \times 0.05$ mm^3. They belong to space group $P2_12_12$ with unit cell axes $a = 146.8$ Å, $b = 81.0$ Å, and $c = 41.1$ Å and one protein monomer in the asymmetric unit. These crystals differ from those obtained with the wild-type protein (*13*) in both space group and unit cell content, although the crystallization conditions are essentially the same.

Table 1: Data Collection and Refinement Statistics

resolution (Å)	1.8
space group	$P2_12_12$
cell axes *a, b, c* (Å)	146,8, 81.0, 41.1
nr of observations	142835
nr unique reflections	45118
completeness (%)[a]	97.6 (99.1)
R_{sym} (%)[a,b]	13.4 (27.3)
nr of protein atoms	3453
nr of water	631
nr of FAD atoms	53
nr of ligand atoms	49
R_{factor} (%)[c]	18.0
R_{free}	21.9
rmsd bond lengths (Å)[d]	0.010
Rmsd bond angles (°)[d]	1.3
Ramachandran analysis[e]	
most favored (%)	93
additionally allowed (%)	7

[a] The values for the highest resolution shell are in parentheses. [b] $R_{sym} = \sum_h\sum_i|I_i(h)\text{-}I(h)|/\sum_h\sum_i I_i(h)$, where $I_i(h)$ and $I(h)$ are the i^{th} and mean measurements, respectively, of reflection *h*. [c] *R*-factor $= \sum_h||Fo|\text{-}|Fc||/\sum_h|Fo|$, where *F*o and *F*c are observed and calculated structure factors, respectively, of reflection *h*. [d] The rmsd from the ideal values were calculated with the program Refmac (*25*). [e] Calculated with Procheck (*32*).

Structure Solution and Refinement. The crystals of FprA−H57Q were soaked in a cryoprotectant solution consisting of 30% (w/v) poly(ethylene glycol) 4000, 0.1 M sodium citrate at pH 5.6, 0.2 M ammonium acetate, 20% (v/v) glycerol, and 0.65 mM $NADP^+$ and flash-cooled in liquid nitrogen. Data were collected at the ID14-EH1 beamline of ESRF (Grenoble), using a MarCCD detector. Data integration was performed by MOSFLM (*23*), whereas merging and scaling were made using the CCP4 program suite (*24*). The structure was determined by molecular replacement with CCP4 programs, via the graphic interface CCP4i. Monomer A of wild-type FprA structure (pdb code 1LQT) was used as a search model. After rigid body fitting, the final solution had a correlation coefficient of 71% and an *R*-factor of 35%. The model was subjected to cycles of restrained refinement by REFMAC (*25*) against all the data up to 1.8 Å and solvent building by the ARP/wARP package (*26*). Electron density maps were inspected and the model manually corrected by the program O (*27*). Refinement and map calculations were carried out against 95% of the data, and 5% randomly omitted reflections were used for the calculation of R_{free} to monitor the refinement protocol (Table 1).

RESULTS

Protein Overproduction and Purification. All FprA forms were produced as *N*-terminal poly-His fusions to obtain the enzyme variants, which are less stable than the wild-type protein, in quantities sufficient for these studies. The recombinant proteins were purified by nickel-chelate chromatography to greater than 90% purity with a yield of about 30%. The spectral and catalytic properties of $(His)_6$FprA or $(His)_6$FprA−H57Q were indistinguishable from those of their counterparts lacking the His-tag. Thus, all functional and structural studies were performed without removing the *N*-terminal extension. Studies on the His57 mutants were performed on 2′,5′ADP Sepharose-purified preparations, which lack any trace of the NADPO-bound enzyme. In this article, the term FprA will be used to indicate the His-tagged form of the enzyme.

Table 2: Steady-State Kinetic Parameters of the FprA Forms in the NADPH−Cytochrome *c* Reductase Reaction, Using Either *M. smegmatis* FdxA or Spinach Leaf Fd I as the Electron Acceptor[a]

M. smegmatis FdxA

FprA form	k_{cat}[b] s^{-1}	K_m^{NADPH} μM	k_{cat}/K_m^{NADPH} $s^{-1}\mu M^{-1}$	K_m^{FdxA} μM	k_{cat}/K_m^{FdxA} $s^{-1}\mu M^{-1}$
wild type	5.6	0.45	12	0.014	400
Glu214Ala	13	0.5	26	0.017	765
His57Ala	7.3	0.15	49	0.49	15
His57Gln	5.2	0.12	43	0.62	8.4

Spinacia oleracea Fd I

FprA form	k_{cat}[b] s^{-1}	K_m^{NADPH} μM	k_{cat}/K_m^{NADPH} $s^{-1}\mu M^{-1}$	$K_m^{Fd\ I}$ μM	$k_{cat}/K_m^{Fd\ I}$ $s^{-1}\mu M^{-1}$
wild type	13	1.0	13	0.53	25
Glu214Ala	10	0.28	36	0.38	26
His57Ala	2.4	0.07	34	2.6	0.92
His57Gln	2.3	0.06	41	3.6	0.64

[a] The activity was assayed at 25 °C in 100 mM Tris-HCl at pH 8.2, using 50 μM cytochrome *c*. All reported values were obtained with a relative standard deviation lower than 10%. [b] The k_{cat} values are expressed as moles of electrons transferred per mole of enzyme (based on FAD content) per second.

Spectral Properties and Thermal Stability. All three FprA variants were isolated in the holoenzyme form. The His57Ala and His57Gln mutants displayed small but significant differences in the visible region of their absorption spectra with respect to that of the wild-type FprA, indicating subtle alterations of the FAD environment. Extinction coefficients (as mM^{-1} cm^{-1}) at the wavelength of absorption maxima (in parentheses) were 11.3 (451 nm), 11.3 (451 nm), 11.0 (449 nm), and 10.9 (448 nm) for wild-type FprA, FprA−E214A, FprA−H57A, and FprA−H57Q, respectively. First-order rate constants for the unfolding of wild-type and mutant enzymes at different temperatures were analyzed using the Eyring plot (Supporting Information, Figure 1). The differences in the activation free energy for the thermal unfolding ($\Delta\Delta G^{\ddagger}_{unfolding}$) at 40 °C between the mutant forms and the wild-type enzyme were −6.4, −7.9 and −5.4 kJ/mol for FprA−E214A, FprA−H57A, FprA−H57Q, respectively.

Steady-State Kinetics. The kinetic parameters of the wild-type FprA and its mutant forms have been determined for the ferredoxin-dependent NADPH-cytochrome *c* reductase reaction using *M. smegmatis* FdxA (*28*) as the substrate. Initial velocity data yielded parallel lines in double reciprocal plots. As shown in Table 2, the Glu214Ala mutation increased the catalytic efficiency (k_{cat}/K_m) of the enzyme for both substrates, mainly because of a doubling in k_{cat}. The mutations of His57 increased the catalytic efficiency for NADPH but greatly decreased it for FdxA because of a 3-fold decrease in the K_m^{NADPH} value and a 40-fold increase in the K_m^{FdxA} value, respectively. With the aim to better understand the large effect of the His57 mutations on K_m^{FdxA}, the enzyme forms were also assayed using spinach leaf Fd I (a 2Fe ferredoxin) as the electron acceptor. The trend observed with FdxA was confirmed, but the $K_m^{Fd\ I}$ of the His57 mutants was increased only 6-fold with respect to that of the wild-type enzyme. Interestingly, the k_{cat}/K_m value for ferredoxin of these mutants was decreased to about 3% of the value of the wild-type enzyme, leading to the conclusion that the oxidative half-reaction is hampered in the FprA His57 mutants (Discussion). To determine the effect of amino acyl substitutions on the reaction between FprA and NADPH, the NADPH−ferricyanide reductase activity of the enzyme forms was investigated. In this assay, initial velocities should be fully limited by the rate of the reductive half-reaction. As shown in Table 3, all mutations mainly affected the k_{cat} value. The effect of the Glu214Ala mutation was moderate, whereas both amino acid changes at position 57 decreased the k_{cat} value by about 5-fold. The kinetic parameters of FprA and FprA−H57Q for the ferricyanide reductase reaction were also determined by substituting NADH for NADPH. The the k_{cat} value of FprA−H57Q in the NADH-dependent reaction (7.5 ± 0.3 e^-eq/s) was decreased in comparison to that of the wild-type enzyme (42 ± 0.9 e^-eq/s) to the same extent as that observed for the NADPH-dependent reaction. The K_m^{NADH} value was only slightly affected by the mutation (29 ± 4 and 68 ± 4 μM for the mutant and wild-type FprA, respectively). Because FprA has a very low affinity for NAD^+ (*10*) (see below), these results suggest that the replacement of His57 impaired the hydride transfer between NAD(P)H and FAD rather than the $NAD(P)^+$ release, which might also cause a slower reductive half-reaction.

Table 3: Steady-State Kinetic Parameters of the FprA Forms in the NADPH−$K_3Fe(CN)_6$ Reductase Reaction[a]

FprA form	k_{cat}[b] s^{-1}	K_m^{NADPH} μM	k_{cat}/K_m^{NADPH} $s^{-1}\mu M^{-1}$
wild type	48	0.60	80
Glu214Ala	26	0.30	87
His57Ala	9	0.41	22
His57Gln	11	0.57	19

[a] The activity was assayed at 25 °C in 100 mM Tris-HCl at pH 8.2. All reported values were obtained with a relative standard deviation lower than 10%. [b] The k_{cat} values are expressed as moles of electrons transferred per mole of enzyme (based on FAD content) per second.

Binding of $NADP^+$ and NAD^+, and Redox Properties of FprA-Bound FAD. The effect of the mutations on the K_m value of FprA for NADPH (and to a lower extent on the K_m value for NADH) prompted us to study the binding of these ligands spectrophotometrically (Supporting Information, Figure 2). For the wild-type and Glu214Ala FprA forms, very similar K_d values were obtained (60 ± 4 and 67 ± 4 μM, respectively). On the contrary, the K_d values obtained for the complexes of FprA−H57A and FprA−H57Q with $NADP^+$ were 24 ± 1 and 16 ± 2 μM, respectively. The binding of $NADP^+$ to His57 mutants also yielded spectral changes significantly more intense than those observed with the wild-type FprA. Similar results were obtained by titrating FprA−H57Q with NAD^+ (not shown). The observed spectral perturbations indicate that the His57Gln and His57Ala substitutions alter the positioning of the $NAD(P)^+$ nicotinamide ring in the active site, thereby increasing its affinity.

Anaerobic photoreduction experiments have been carried out to define the spectral properties of the flavin prosthetic group in its various redox states for the subsequent interpretation of the rapid-kinetic studies. The photoreduction of wild-type FprA proceeded from oxidized to fully reduced FAD without the transient accumulation of any intermediate species, as already reported for untagged FprA (*10*) (not shown). All FprA mutants behaved in a manner similar to that of the wild-type protein. As previously reported (*10*), the presence of NADP(H) during the photoreduction of the wild-type enzyme (Figure 2A) stabilized the SQ and an intermediate species characterized by an absorbance band

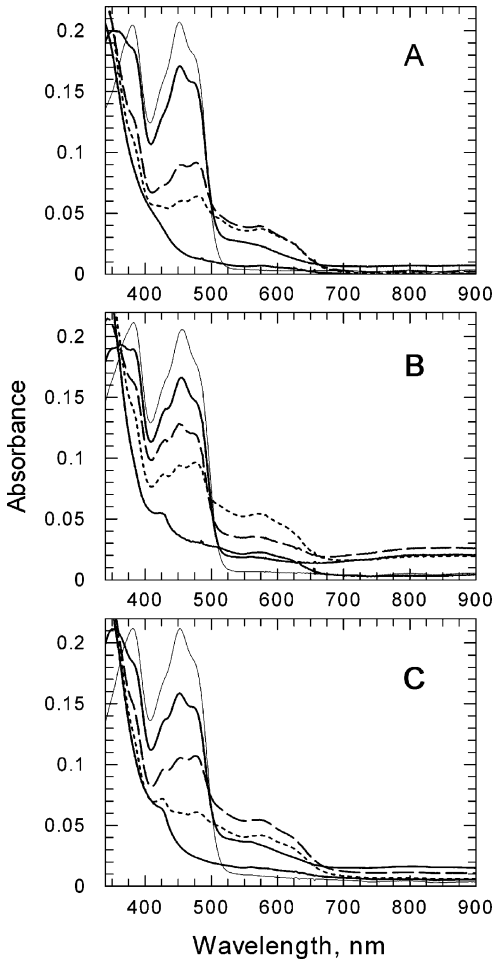

FIGURE 2: Photoreduction of FprA forms in the presence of $NADP^+$. Absorbance spectra of anaerobic FprA solutions (ca. 18 μM), in the presence of a slight excess of $NADP^+$, recorded before (thin lines) and after successive periods of illumination. The solutions included 10 mM HEPES−NaOH at pH 7.0, 100 mM NaCl, 10% glycerol, 1.4 μM 5-deazariboflavin, and 15 mM EDTA. (A) FprA; (B) FprA−H57Q; (C) FprA−E214A.

centered at 550 nm, identified as a charge-transfer complex between NADPH and the oxidized enzyme (CT1) (*10*). The photoreduction of FprA−H57A or FprA-H75Q in the presence of NADP(H) also led to the formation of the SQ. However, the spectrum of the charge-transfer species, which accumulated during the early phases of reduction, was markedly different from that of the wild-type enzyme, showing low absorbance at 550 nm and a very broad band with a maximum at about 850 nm (Figure 2B). This species could be attributed to a charge-transfer complex involving fully reduced FAD and $NADP^+$ (CT2) (*10*). The behavior of the Glu214Ala mutant was intermediate between those of the wild-type enzyme and the His57 mutant forms, displaying a mixture of CT1 and CT2 (Figure 2C). The redox titrations performed at pH 7.0 using antraquinone-2,6-disulfonate as the redox indicator yielded E_m values of -192 ± 0.2 and -203 ± 1.2 mV for the oxidized/dihydroquinone FAD couple of FprA and FprA−H57Q, respectively (Supporting Information, Figure 3). These E_m values were confirmed using a more negative indicator (antraquinone-2-sulfonate). The value we obtained for the E_m of wild-type FprA (both tagged and untagged) is significantly less negative than that determined by McLean and co-workers (*29*) (-230 ± 12 mV). We can conclude that the His57Gln mutation has a small but significant effect on the E_m value of the FprA-bound FAD, making it more negative by ca. 10 mV.

Table 4: Comparison of Rate Constants for the Hydride Transfer between NADPH or NADH and Enzyme-Bound FAD with k_{Cat} Values in the NADPH−Ferricyanide Reaction[a]

FprA form	k_{HT}^{NADPH} s^{-1}	k_{HT}^{NADH} s^{-1}	k_{cat}[b] s^{-1}
wild type	36	36	43
His57Gln	9.4	7.4	7

[a] All rate constants are expressed as moles of electrons transferred per mole of enzyme (based on FAD content) per second. Both rapid-reaction and steady-state kinetic measurements were performed at 25 °C in 50 mM HEPES−NaOH at pH 7.0, containing 100 mM NaCl and 10% glycerol. [b] The k_{cat} values were obtained with a relative standard deviation lower than 10%.

Scheme 1

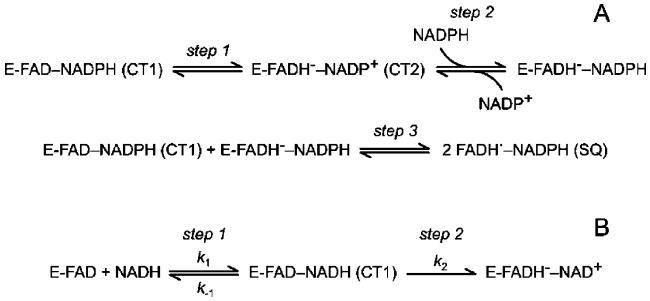

Rapid-Reaction Studies of the Reductive Half-Reaction. To test the hypothesis that the substitution of His57 with neutral residues lowers the rate of hydride transfer, flavin reduction by either NADPH or NADH in the His57Gln mutant and in the wild-type FprA was studied by stopped-flow spectrophotometry. To avoid FAD loss from FprA−H57Q, fast kinetics were performed under conditions that differed from those used in steady-state studies. To allow for comparison, the k_{cat} values for the NADPH−ferricyanide reaction were also determined at pH 7 (Table 4). The reaction of the wild-type FprA with 1 mM NADPH is shown in Figures 3A and 4A. The spectrum recorded immediately after mixing displayed an absorbance at 450 nm, lower than that expected for oxidized FprA, even when taking into account the instrument dead-time and a broad absorbance band around 530 nm. Then, a further bleaching of the 450-nm band occurred, with a parallel decrease of the A_{530}. Absorbance traces at different wavelengths fitted well to a single-exponential decay equation yielding essentially the same apparent rate constant (k_{obs}) of 18 ± 0.4 s^{-1}. Therefore, the formation of a substantial amount of CT1 took place within the instrument dead time, and the observable part of the reaction corresponded to the conversion of CT1 to CT2 via hydride transfer followed by the rapid exchange of NADPH for $NADP^+$ to yield the reduced FprA/NADPH complex, until an equilibrium state was reached (Scheme 1A, steps 1 and 2). Because the latter exchange reaction is thermodynamically favored and is faster than hydride transfer, no CT2 species was observed during the process. On a longer timescale (not shown), the SQ species accumulated (Scheme 1A, step 3). Lowering the NADPH concentration resulted in a progressive increase of k_{obs}, as already reported (*29*), and rationalized on the basis of the NADPH/$NADP^+$ exchange reaction (*30*). The reduction of FprA−H57Q by NADPH differed from that of the wild-type FprA in three aspects

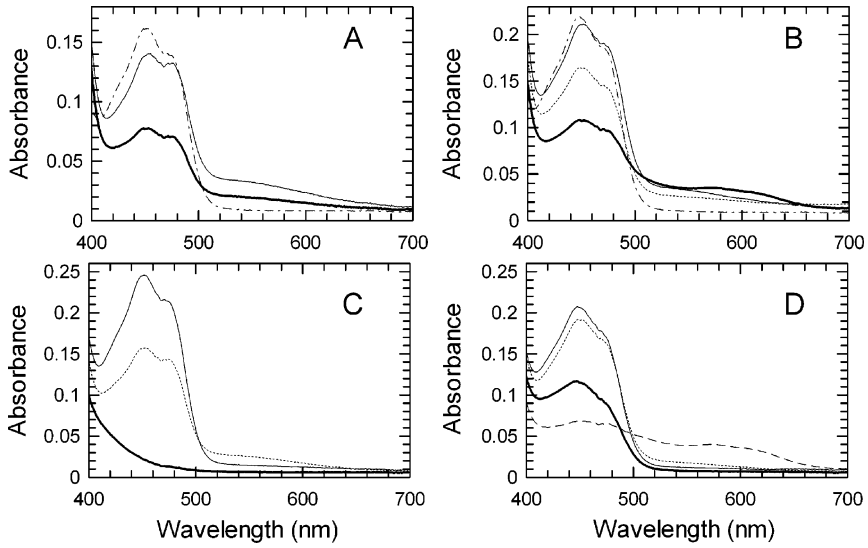

FIGURE 3: Selected spectra recorded by stopped-flow spectrophotometry during the anaerobic reduction of FprA and FprA−H57Q by NADPH and NADH. All reactions were carried out at 25 °C in 50 mM HEPES−NaOH at pH 7.0, containing 100 mM NaCl and 10% glycerol. (A) Reaction of FprA (ca. 14 μM, after mixing) with NADPH (ca. 1 mM, after mixing): thin line, spectrum recorded immediately after mixing; thick line, spectrum recorded at 0.5 s; dash−dot line, spectrum of oxidized enzyme. (B) Reaction of FprA−H57Q (ca. 14 μM, after mixing) with NADPH (ca. 1 mM, after mixing): thin line, spectrum recorded immediately after mixing; dotted line, spectrum recorded at 150 ms; thick line, spectrum recorded at 1.9 s; dash−dot line, spectrum of oxidized enzyme. (C) Reaction of FprA (ca. 20 μM, after mixing) with NADH (ca. 0.2 mM, after mixing): thin line, spectrum recorded immediately after mixing; dotted line, spectrum recorded at 47 ms; thick line, spectrum recorded at 1 s. (D) Reaction of FprA−H57Q (ca. 20 μM, after mixing) with NADH (ca. 0.2 mM, after mixing): thin line, spectrum recorded immediately after mixing; dotted line, spectrum recorded at 47 ms; thick line, spectrum recorded at 1 s; dashed line, spectrum recorded at 100 s. The spectra of oxidized enzyme forms were omitted in the lower panels because they were superimposable on those recorded immediately after mixing.

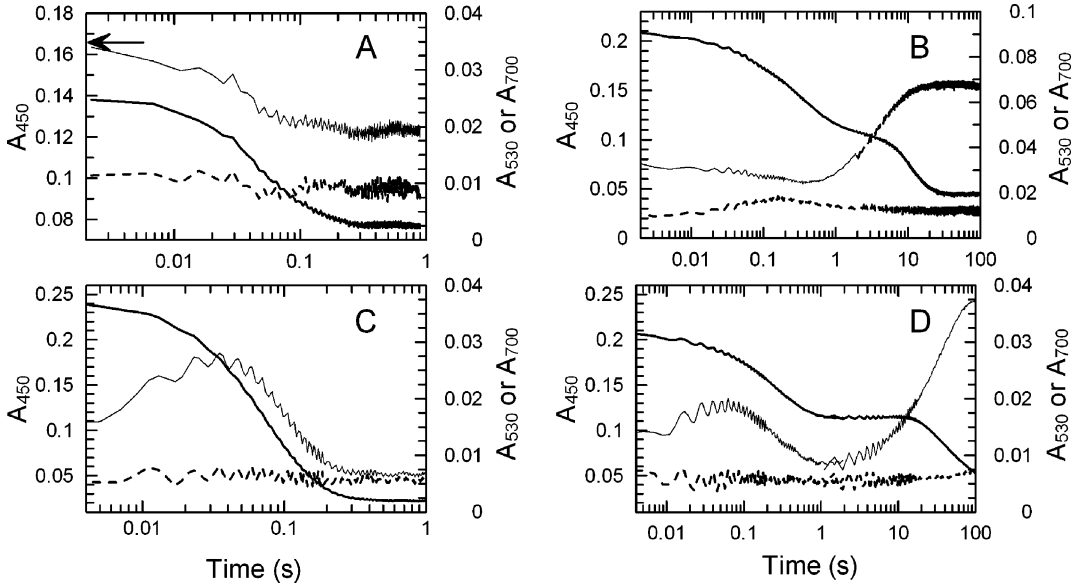

FIGURE 4: Time courses of the anaerobic reduction of FprA and FprA−H57Q by NADPH and NADH, monitored by stopped-flow spectrophotometry. The experimental conditions are reported in the legend for Figure 4. Thick lines, the absorbance at 450 nm; thin lines, the traces at 530 nm; dashed lines, traces at 700 nm. The traces recorded from different shots over different time intervals (0.002−1 and 1−100 s) were combined in the same plot. (A) Reaction of FprA with NADPH. The arrow indicates the expected initial A_{450} value. (B) Reaction of FprA−H57Q with NADPH. (C) Reaction of FprA with NADH. (D) Reaction of FprA−H57Q with NADH.

(Figures 3B and 4B). First, the reaction of FprA−H57Q with NADPH was much slower, leading to some overlap between reduction and SQ formation. Second, the amount of CT1 observed immediately after mixing was smaller. Third, a transient increase of A_{700} was observed and interpreted as the build up of CT2. The global fitting of the data set recorded over the entire absorbance range allowed the deconvolution of the process in two exponential decays, with apparent rate constants, k_{obs1} and k_{obs2}, of 4.7 ± 0.1 and 0.3 ± 0.09 s^{-1}, respectively. The spectra recorded at selected time points during the reaction (Figure 3B) indicated that the fast phase corresponded to enzyme reduction (Scheme 1A, steps 1 and 2), whereas the slower one to SQ formation (Scheme 1A, step 3).

Because no SQ was detected during the titration of FprA with NADH (*10*), thus simplifying the reaction, the FprA forms were also reacted with NADH. The absorbance traces of wild-type FprA were biphasic at all wavelengths (Figure 4C) with the fast phase corresponding to CT1 formation (Scheme 1B, step 1) and the slower phase associated with

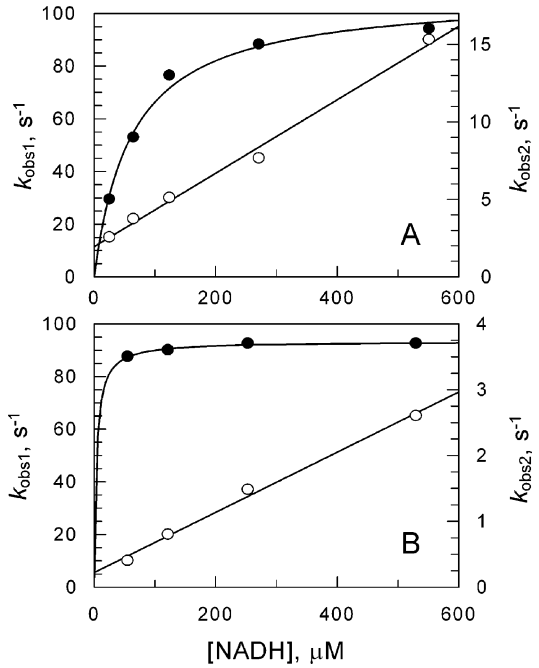

FIGURE 5: Concentration dependence of the apparent rate constants for the reduction of FprA and FprA−H57Q by NADH. The reaction conditions are reported in the legend of Figure 4. (○), k_{obs1}; (●), k_{obs2}. The fitted curves are a straight line and a rectangular hyperbola, respectively. (A) FprA; (B) FprA−H57Q.

flavin reduction (Scheme 1B, step 2). As expected (*10*), no SQ species was detected even at very long reaction times (Figure 3C). The apparent rate constants of the fast phase (k_{obs1}) increased linearly with NADH concentration, whereas the NADH dependence of the slower phase (k_{obs2}) was hyperbolic (Figure 5A). This behavior agrees well with that previously reported for AdR and can thus be analyzed with the same model (*31*):

$$k_{obs1} = k_1[\text{NADH}] + k_{-1} + k_2 \quad (1)$$

$$k_{obs2} = (k_1 k_2[\text{NADH}])/(k_1[\text{NADH}] + k_{-1} + k_2) \quad (2)$$

The slope of the linear plot of k_{obs1} versus the NADH concentration (eq 1) yielded a value of $1.4 \times 10^5 \pm 7 \times 10^3$ M^{-1} s^{-1} for the second-order rate constant k_1. The upper limit of the hyperbolic plot of k_{obs2} versus the NADH concentration (eq 2) yielded a value of 18 ± 0.7 s^{-1} for the hydride-transfer rate constant k_2, identical to that obtained with NADPH. The reaction of FprA−H57Q with NADH occurred in three phases (Figures 3D and 4D). The first observable phase consisted of CT1 formation. The plot of k_{obs1} versus NADH concentration was linear (Figure 5B). Equation 1 yielded a value of $1.1 \times 10^5 \pm 7 \times 10^3$ M^{-1} $s^{-1}$for the second-order rate constant k_1 for CT1 formation, which is similar to that observed for the wild-type FprA. The subsequent hydride-transfer step was slower than that in the case of the wild-type enzyme and did not lead to complete enzyme reduction (Figures 3D and 4D). The apparent rate constant of the second phase (k_{obs2}) was poorly dependent on NADH concentration (Figure 5B). The application of eq 2 yielded an upper limit of 3.7 ± 0.02 s^{-1} for k_{obs2}. This value matched well that obtained with NADPH (4.7 ± 0.1 s^{-1}). At longer times, the formation of SQ was observed (Figures 3D and 4D). Thus, the mechanism of the NADH reduction of FprA−H57Q differed from that of the wild-type FprA in two aspects. First, the hydride-transfer reaction was not irreversible, leading to an equilibrium mixture containing a substantial amount of the CT1 species even at NADH concentration up to 500 μM. Second, the partially reduced mutant enzyme was slowly converted to the SQ species. In conclusion, NADH seemed to act on FprA−H57Q in an NADPH-like manner, resulting in only a partial FAD reduction and in the stabilization of the SQ of the enzyme-bound flavin. We propose that this behavior is the result of a stronger interaction of the mutant with NAD(H).

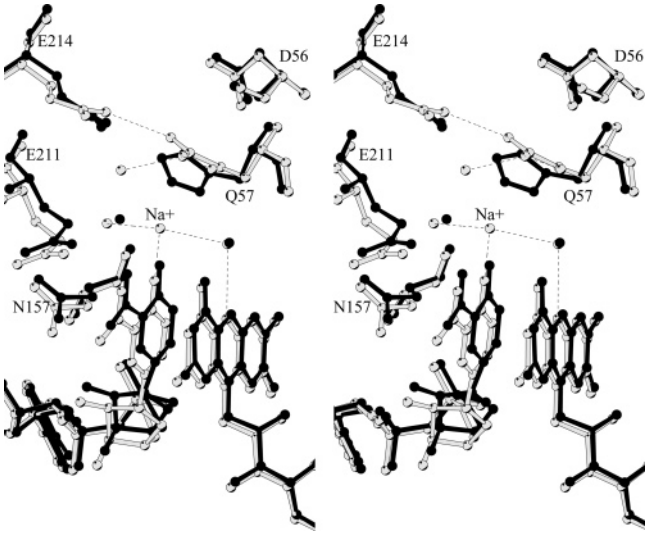

FIGURE 6: Comparison of the active-site structures of FprA−H57Q and wild-type FprA. A stereo plot of the structure of FprA−H57Q (open bonds) overlaid on that of the wild-type enzyme (closed bonds), showing the 4-oxo derivative of $NADP^+$ (NADPO) bound to the active site of both enzyme forms. The H bonds are depicted as dashed lines. The structure of the FprA−NADPO complex (pdb entry 1LQT) has been described elsewhere (*13*).

As summarized in Table 4, the rate constants for hydride transfer from either NADPH or NADH to FAD in FprA and in FprA−H57Q are very close to their corresponding turnover numbers, determined under steady-state conditions. This demonstrates that (i) hydride transfer is the rate-limiting step of the ferricyanide reductase reaction both in wild-type FprA and mutant species and (ii) the lower ferricyanide reductase activity of FprA−H57Q is the result of the impairment of the hydride transfer step of the catalytic cycle.

Three-Dimensional Structure of FprA−H57Q. The His57Gln mutant protein crystallizes under the same conditions as the wild-type form but in a different crystal form. Therefore, molecular replacement had to be employed for structure solution (Table 1). The overall structure of FprA−H57Q is very similar to that of the wild-type (*13*) as indicated by a rms deviation of 0.54 Å for 452 equivalent Cα atoms (Supporting Information, Figure 4). The enzyme crystallizes in the same dimeric form as the wild-type species with the only difference that the two monomers are related by a crystallographic (rather than noncrystallographic) 2-fold axis. The His57Gln mutation does not cause any large changes in the active site geometry (Figure 6). The Cβ, Cδ, and Nϵ2 atoms of the Gln57 side chain superimpose on the Cβ, Cδ2, and Nϵ2 atoms of the wild-type His57 side chain. The Oϵ1 atom of Gln57 is engaged in H bonds with two ordered water molecules. An inspection of the electron density unambigu-

ously indicates that the nicotinamide ring of the bound $NADP^+$ is modified by the addition of an oxygen atom bound to the C4 carbon. This finding also shows that the mutant, like the wild-type, catalyzes the formation of NADPO. In the mutant structure, the nicotinamide ring is shifted by about 0.7 Å. This movement does not affect the distance between flavin N5 and nicotinamide C4 atoms (which remains 3.3 Å), but it slightly alters the geometry of the nicotinamide−flavin interactions. The flavin N10-flavin N5-nicotinamide C4 angle changes from 104° observed in the wild-type enzyme to 95° in the mutant form. Also, the solvent structure is remarkably well-conserved, including an ordered water molecule that is H bonded to the flavin N5 atom and a water molecule that interacts (3.5 Å distance) with the oxygen atom of the modified nicotinamide ring. With respect to the wild-type FprA, there is an additional well-defined electron density peak located between Gln57 and the nicotinamide ring. The peak is located at 2.2 and 2.3 Å distance from the NADPO oxygen and the Asp161 Oδ1 atoms, respectively; it has been interpreted as a tightly bound sodium ion (Figure 6), the B-factor of which has a value of 14 $Å^2$ in the refined model.

DISCUSSION

Mutations targeting residues His57 and Glu214 of FprA had only moderate effects on the catalytic properties of the enzyme, allowing an extensive survey of the altered features of the protein variants. Thus, we could provide a detailed picture of the reductive half-reaction of the enzyme, describing the mechanism of bound-FAD reduction by either NADPH or NADH and identifying the reaction intermediates involved. These results provide a framework for interpreting the properties of other enzymes of the GR-type FNR family.

All mutations resulted in a mild destabilization of the protein, which can be explained by the removal of the His57/Glu214 ion pair at the interface between the protein domains where the active-site crevice is located. The impact of the Glu214Ala mutation on the kinetic properties of FprA is negligible. Thus, the following discussion will focus on the analysis of the properties of the wild-type FprA compared to those of the His57 variants. The catalytic mechanism of FprA in the reduction of ferredoxin by NADPH is quite complex (*10*), and the effects of the mutations on the catalytic parameters of the enzyme in this reaction are difficult to interpret. The major effect of the His57Ala and His57Gln substitutions was on the catalytic efficiencies with either FdxA or Fd I as the electron acceptor. Clearly, electron transfer from the reduced enzyme to ferredoxin was impaired in these mutant forms. Further analysis of the oxidative portion of the catalytic cycle by presteady-state kinetics was prevented by the unavailability of FdxA in sufficient amounts. Additional studies, specifically targeting electron transfer between FprA and FdxA, will be planned for the near future. The 5-fold decrease of the k_{cat} value for either NADPH or NADH in the ferricyanide reductase reaction suggested a specific effect of the His57 substitutions on the reductive half-reaction of FprA. Rapid-reaction studies using NADPH or NADH as the reductant unequivocally indicated that the hydride transfer was the step affected by the His57Gln mutation. This limited (5-fold) but significant effect on the hydride-transfer rate correlates well with difference spectrophotometry data, which revealed small alterations in the positioning in the active site of the nicotinamide moiety of enzyme-bound $NADP^+$ as well as with the active-site geometry differences observed in the crystal structure of the NADPO complex of the His57Gln variant in comparison to those of the wild-type FprA. Titration studies also showed that the His57 mutants exhibited a significantly increased affinity for the $NAD(P)^+$ product. Thus, His57 has a role in modulating the enzyme affinity for $NAD(P)^+$ and in the precise positioning of the nicotinamide ring in the active site. As a result of the increased affinity for $NADP^+$, the His57 substitutions also caused an increased stability of the CT2 species as observed in photoreduction and stopped-flow experiments. It is likely that the side chain of His57 favors $NAD(P)^+$ replacement by NAD(P)H during the catalytic cycle (Scheme 1), presumably because of the electrostatic repulsion between the positively charged His57 side chain and the (also positively charged) nicotinamide ring of the oxidized pyridine nucleotide. Finally, rapid kinetic experiments showed that the His57 replacements increased the SQ stability. Indeed, NADH was found to induce SQ formation in FprA−H57Q but not in wild-type FprA. This finding correlates with the increased affinity for NAD^+ of the His57Gln variant in comparison to that of the wild-type FprA, which also makes NADH unable to fully reduce the mutant enzyme. Thus, the His57Gln mutation makes NAD(H) mimic NADP(H). In conclusion, the previous hypothesis that His57 is required for the thermodynamic stabilization of the FAD semiquinone in FprA can be rejected. Moreover, although we could not rule out the role of His57 in favoring proton exchanges between flavin and the solvent during ferredoxin reduction, His57 does not seem to be involved in FAD reoxidation by ferricyanide. Given the critical role established here for the precise geometry of the nicotinamide−isoalloxazine interaction in the FprA catalytic mechanism, a function more crucial than that played by His57 in the catalysis of hydride transfer may be foreseen for residues Glu211 and Asp161 (Figure 1).

SUPPORTING INFORMATION AVAILABLE

Eyring plots of the thermal unfolding of the enzyme forms, spectrophotometric titration of the FprA forms with $NADP^+$, Nernst plots of the redox titration of the FAD cofactor in FprA and FprA−H57Q, and the overall crystal structure of FprA−H57Q. This material is available free of charge via the Internet at http://pubs.acs.org.

REFERENCES

1. Ceccarelli, E. A., Arakaki, A. K., Cortez, N., and Carrillo, N. (2004) Functional plasticity and catalytic efficiency in plant and bacterial ferredoxin-NADP(H) reductases, *Biochim. Biophys. Acta 1698*, 155−156.
2. Zanetti, G., and Aliverti, A. (2004) Ferredoxin-$NADP^+$ reductase, in *Encyclopedia of Biological Chemistry* (Lennarz, W. J., and Lane, M. D., Eds.) Vol. 2, pp 107−111, Academic Press, Elsevier, New York.
3. Arakaki, A. K., Ceccarelli, E. A., and Carrillo, N. (1997) Plant-type ferredoxin-$NADP^+$ reductases: a basal structural framework and a multiplicity of functions, *FASEB J. 11*, 133−140.
4. Lambeth, J. D., Seybert, D. W., Lancaster, J. R., Jr, Salerno, J. C., and Kamin, H. (1982) Steroidogenic electron transport in adrenal cortex mitochondria, *Mol. Cell. Biochem. 45*, 13−31.
5. Hanukoglu, I. (1992) Steroidogenic enzymes: structure, function, and role in regulation of steroid hormone biosynthesis, *J. Steroid Biochem. Mol. Biol. 43*, 779−804.

6. Lill, R., and Muhlenhoff, U. (2005) Iron-sulfur-protein biogenesis in eukaryotes, *Trends Biochem Sci. 30*, 133−141.
7. Li, J., Saxena, S., Pain, D., and Dancis, A. (2001) Adrenodoxin reductase homolog (Arh1p) of yeast mitochondria required for iron homeostasis, *J. Biol. Chem. 276*, 1503−1509.
8. Lange, H., Kaut, A., Kispal, G., Lill, R. (2000) A mitochondrial ferredoxin is essential for biogenesis of cellular iron-sulfur proteins, *Proc. Natl. Acad. Sci. U.S.A. 97*, 1050−1055.
9. Cole, S. T., Brosch, R., Parkhill, J., Garnier, T., Churcher, C., Harris, D., Gordon, S. V., Eiglmeier, K., Gas, S., et al. (1998) Deciphering the biology of *Mycobacterium tuberculosis* from the complete genome sequence, *Nature 393*, 537−544.
10. Fischer, F., Raimondi, D., Aliverti, A., and Zanetti, G. (2002) *Mycobacterium tuberculosis* FprA, a novel bacterial NADPH-ferredoxin reductase, *Eur. J. Biochem. 269*, 3005−3013.
11. Carrillo, N., and Ceccarelli, E. A. (2003) Open questions in ferredoxin-$NADP^+$ reductase catalytic mechanism, *Eur. J. Biochem. 270*, 1900−1915.
12. Karplus, P. A., and Faber, H. R. (2004) Structural aspects of plant ferredoxin: $NADP^+$ oxidoreductases, *Photosynth. Res. 81*, 303−315.
13. Bossi, R. T., Aliverti, A., Raimondi, D., Fischer, F., Zanetti, G., Ferrari, D., Tahallah, N., Maier, C. S., Heck, A. J. R., Rizzi, M., and Mattevi, A. (2002) A covalent modification of $NADP^+$ revealed by the atomic resolution structure of FprA, a *Mycobacterium tuberculosis* oxidoreductase, *Biochemistry 41*, 8807−8818.
14. Ziegler, G. A., Vonrhein, C., Hanukoglu, I., and Schulz, G. E. (1999) The structure of adrenodoxin reductase of mitochondrial P450 systems: electron transfer for steroid biosynthesis, *J. Mol. Biol. 289*, 981−990.
15. Ziegler, G. A., and Schulz, G. E. (2000) Crystal structures of adrenodoxin reductase in complex with $NADP^+$ and NADPH suggesting a mechanism for the electron transfer of an enzyme family, *Biochemistry 39*, 10986−10995.
16. Müller, J. J., Lapko, A., Bourenkovi, G., Ruckpaul, K., and Heinemann, U. (2001) Adrenodoxin reductase-adrenodoxin complex structure suggests electron-transfer path in steroid biosynthesis, *J. Biol. Chem*. 276, 2786−2789.
17. Brandt, M. E., and Vickery, L. E. (1993) Charge pair interactions stabilizing ferredoxin-ferredoxin reductase complexes. Identification by complementary site-specific mutations, *J. Biol. Chem. 268*, 17126−17130.
18. Piubelli, L., Aliverti, A., Bellintani, F., Zanetti, G. (1995) Spinach ferredoxin I: overproduction in *Escherichia coli* and purification, *Protein Expression Purif. 6*, 298−304.
19. Aliverti, A., Curti, B., and Vanoni, M. A. (1999) Identifying and quantitating FAD and FMN in simple and iron-sulfur-containing flavoproteins, in *Methods in Molecular Biology*, *Flavoprotein Protocols* (Chapman, S. K., and Reid, G. A., Eds.) Vol. 131, pp 9−23, Humana Press Inc., Totowa, NJ.
20. Wang, Z. X., Kumar, N. R., and Srivastava, D. K., (1992) A novel spectroscopic titration method for determining the dissociation constant and stoichiometry of protein−ligand complex, *Anal. Biochem. 206*, 376−381.
21. Massey, V., and Hemmerich, P. (1977) A photochemical procedure for reduction of oxidation−reduction proteins employing deazariboflavin as catalyst, *J. Biol. Chem. 252*, 5612−5614.
22. Clark, W. M. (1960) in *Oxidation−Reduction Potentials of Organic Systems*, Williams and Wilkins Co., Baltimore.
23. Leslie, A. G. W. (1999) Integration of macromolecular diffraction data, *Acta Crystallogr., Sect. D 55*, 1696−1702.
24. Collaborative Computational Project, Number 4. (1994) The CCP4 suite: programs for protein crystallography, *Acta Crystallogr, Sect. D 50*, 760−767.
25. Murshudov, G. N., Vagin, A. A., Dodson, E. J. (1997) Refinement of macromolecular structures by the maximum-likelihood method, *Acta Crystallogr, Sect. D 53*, 240−255.
26. Morris, R. J., Perrakis, A., and Lamzin, V. S. (2002) ARP/wARP's model-building algorithms. I. The main chain, *Acta Crystallogr, Sect. D 58*, 968−975.
27. Jones, T. A., Zou, J. Y., Cowan, S. W., and Kjeldgaard, M. (1991) Improved methods for building protein models in electron density maps and the location of errors in these models, *Acta Crystallogr, Sect. A 47*, 110−119.
28. Imai, T., Matsumoto, T., Ohta, S., Ohmori, D., Suzuki, K., Tanaka, J., Tsukioka, M., and Tobari, J. (1983) Isolation and characterization of a ferredoxin from *Mycobacterium smegmatis* Takeo, *Biochim. Biophys. Acta 743*, 91−97.
29. McLean, K. J., Scrutton, N. S., and Munro, A. W. (2003) Kinetic, spectroscopic and thermodynamic characterization of the *Mycobacterium tuberculosis* adrenodoxin reductase homologue FprA, *Biochem. J. 372*, 317−327.
30. Daff, S. (2004) An appraisal of multiple NADPH binding-site models proposed for cytochrome P450 reductase, NO synthase, and related diflavin reductase systems, *Biochemistry 43*, 3929−3932.
31. Sugiyama, T., Miura, R., and Yamano, T. (1979) Differences between the reactivities of two pyridine nucleotides in rapid reduction process and the reoxidation process of adrenodoxin reductase, *J. Biochem. 86*, 213−223.
32. Laskowski, R. A., MacArthur, M. W., Moss, D. S., and Thornton, J. M. (1993) PROCHECK: a program to check the stereochemical quality of protein structures, *J. Appl. Crystallogr. 26*, 283−291.

BI060369M